Magnetoelastic coupling and microstructure dynamics associated with spin-orbit coupling in the ferrimagnetic/ferroelastic ordered double perovskite Ba_2FeReO_6

Dexin Yang [1,*], Jining Zhou [1], Juan Hu,[1,2] Dexuan Huo,[1] Xuefeng Zhang,[1,2,†] and Michael A. Carpenter [3]

[1]*Institute of Advanced Magnetic Materials; Key Laboratory of Novel Materials for Sensor of Zhejiang Province, College of Materials and Environmental Engineering, Hangzhou Dianzi University, Hangzhou 310018, China*

[2]*Key Laboratory for Anisotropy and Texture of Materials (MOE), School of Materials Science and Engineering, Northeastern University, Shenyang 110819, China*

[3]*Department of Earth Sciences, University of Cambridge, Downing Street, Cambridge CB2 3EQ, United Kingdom*

(Received 22 November 2022; revised 22 March 2023; accepted 30 March 2023; published 20 April 2023)

Strain coupling and relaxation dynamics associated with the ferrimagnetic/ferroelastic phase transition at $T_c \approx 310$ K in double perovskite Ba_2FeReO_6 with a high degree of Fe/Re order have been investigated with resonant ultrasound spectroscopy through the temperature interval ~5–600 K and with applied magnetic field of up to ±2 T. Strain analysis using diffraction data from the literature is consistent with a Landau model of the transition as $Fm\bar{3}m1' \rightarrow I4/mm'm'$, improperly ferroelastic, driven by a magnetic order parameter with symmetry Γ_4^+. Ferroelastic shear strain of up to ~0.0015 arises from spin/orbit coupling and is smaller than is typical of coupling with octahedral tilting. It provides the underlying cause of softening of the shear modulus observed over an interval of ~100 K below T_c, though with order/disorder rather than displacive character for the transition. Hysteretic effects suggest that precursor microstructures and mixed magnetic/ferroelastic domains below T_c depend on the thermal history of the sample and can evolve on a timescale of hours and days at room temperature. Elasticity data collected as a function of external magnetic field reveal that poled samples are slightly softer than those with multiple magnetic domains at 4 K. At 300 K there is a time-dependent viscous component of the response to the field that relates to the bulk modulus and, hence, to volume changes associated with magnetic ordering. A loss peak seen ~20–50 K below T_c in AC magnetic measurements made at frequencies of 0.2–1 kHz yielded an activation energy ~0.4 eV and has been attributed to freezing of magnetic/ferroelastic domain walls. No equivalent loss peak was seen in the acoustic data measured at ~100–500 kHz, however, implying that these domain walls are mobile in response to a dynamic magnetic field on a timescale of $\sim 10^{-2}$–10^{-3} s but immobile in response to a dynamic stress field applied on a timescale of $\sim 10^{-5}$–10^{-6} s. Debye-like acoustic loss peaks at temperatures below ~100 K yielded activation energies of ~0.02–0.1 eV and are discussed in terms of pinning/freezing of polarons. Ba_2FeReO_6 is a material with magnetoelastic and magnetoelectric heterogeneities that might be tuned by choice of thermal history and cation order.

DOI: 10.1103/PhysRevB.107.144108

I. INTRODUCTION

Among the many families of perovskites which have attracted close attention for their phenomenologically rich physics and potential device applications are double perovskites, $A_2BB'O_6$, where one of the B cations is magnetic. In the case of phases with A = Ca, Sr, Ba, B = Cr, Mn, Fe, Co, B′ = Mo, Re, W, the focus has been on combinations of metallic/half-metallic transport properties and magnetism which can be tuned by choices of composition and degree of B/B′ order [1]. The interplay between electronic structure and magnetism in these phases gives rise to paramagnetic–antiferromagnetic/ferromagnetic/ferrimagnetic transitions which may involve coupling with symmetry breaking shear strains, making them also ferroelastic. Some have additional ferroelastic transitions driven by octahedral tilting which add to their interest in the wider context of double perovskites with multiferroic properties [2–5]. A further context relates to the structure and properties of domain walls associated with each type of phase transition for "domain wall nanoelectronics" in which "the wall is the device" [6]. Domain walls in the double perovskites reviewed by Serrate *et al.* [1] can be purely ferroelastic, with local gradients in shear strain, purely magnetic, with local gradients in magnetic moment or simultaneously ferroelastic and magnetic, with coupled gradients of shear strain and moment. This contrasts with the more common combination of coupled gradients in shear strain and electric dipoles such as occurs in the classic single perovskite $BaTiO_3$ which is both ferroelastic and ferroelectric.

The primary objective of the present study was to determine the role of strain coupling and strain relaxation dynamics in the double perovskite, Ba_2FeReO_6 (BFRO), which is ferrimagnetic at room temperature. There are no octahedral tilting transitions, but the ferrimagnetic structure is ferroelastic due to weak spin-orbital coupling. Evidence for significant magnetoelastic coupling has already been provided through the observation by Li *et al.* [7] of substantial softening of the shear

*dy263@hdu.edu.cn
†zhang@hdu.edu.cn

modulus below the transition point. Spin-orbital coupling in double perovskites can be considered at a purely local scale for particular spin and orbital configurations of the B and B′ cations. However, phase transitions are collective phenomena effectively being driven by coupled magnetic and structural order parameters which acquire long correlations. As a consequence, the overall patterns of behavior at a macroscopic scale conform to mean-field models based on coupling between order parameters and their formal coupling with strain. This approach has recently been applied to combined magnetic and tilting transitions in Sr_2FeMoO_6 (SFMO) [8], La_2NiMnO_6 (LNMO) [9], and La_2FeMnO_6 (LFMO) [10], for example.

A formal strain/order parameter coupling model is introduced and tested using diffraction data from the literature. Elastic and anelastic anomalies observed by resonant ultrasound spectroscopy (RUS), with and without an applied magnetic field, are used to characterize elastic relaxations which can occur on timescales from $\sim 10^{-6}$ seconds to hours and days. It is proposed that BFRO contains a variety of heterogeneities related to transformation microstructures, with different combinations of gradients in shear strain and magnetic order that might potentially be manipulated by choice of thermal and magnetic history.

II. FERRIMAGNETIC/FERROELASTIC COUPLING

The paramagnetic-ferrimagnetic transition in BFRO occurs at ~315 K [11–13]. Early diffraction studies gave the structure at room temperature as being cubic [11], and full refinements in space group $Fm\bar{3}m$ showed up to ~97%–98% order of Fe and Re between B and B′ sites [14,15]. Higher resolution diffraction data revealed that the magnetic transition is accompanied by a small tetragonal distortion to a structure in crystallographic space group $I4/mmm$ [16,17]. The magnetic structure shown in Fig. 1 of Plumb *et al.* [18] and Cook and Paramekanti [19] conforms to magnetic space group $I4/mm'm'$.

From the ISOTROPY Software Suite at Brigham Young University [20], the active representation for the symmetry change $Fm\bar{3}m1' \rightarrow I4/mm'm'$ is $\mathrm{m}\Gamma_4^+$. A simple Landau expansion to describe the transition, including coupling with strain, is

$$\begin{aligned} G = {} & \tfrac{1}{2}a(T - T_c)\left(m_1^2 + m_2^2 + m_3^2\right) + \tfrac{1}{4}b\left(m_1^2 + m_2^2 + m_3^2\right)^2 \\ & + \tfrac{1}{4}b'\left(m_1^4 + m_2^4 + m_3^4\right) + \lambda_1\left(m_1^2 + m_2^2 + m_3^2\right)e_a \\ & + \lambda_2\left[\sqrt{3}\left(m_1^2 - m_2^2\right)e_o + \left(m_1^2 + m_2^2 - 2m_3^2\right)e_t\right] \\ & + \lambda_3(m_1m_2e_6 + m_1m_3e_5 + m_2m_3e_4) \\ & + \tfrac{1}{4}\left(C_{11}^o - C_{12}^o\right)\left(e_t^2 + e_o^2\right) + \tfrac{1}{6}(C_{11}^o + 2C_{12}^o)e_a^2 \\ & + \tfrac{1}{2}C_{44}^o\left(e_4^2 + e_5^2 + e_6^2\right). \end{aligned} \tag{1}$$

G is the excess free energy, a, b, b' are standard Landau coefficients, T_c is the critical temperature, λ_1, λ_2, and λ_3 are coupling coefficients and C_{ik}^o are elastic constants of the parent cubic structure. The orientation of the three components order parameter chosen here has $m_1 = m_2 = 0$, $m_3 \neq 0$.

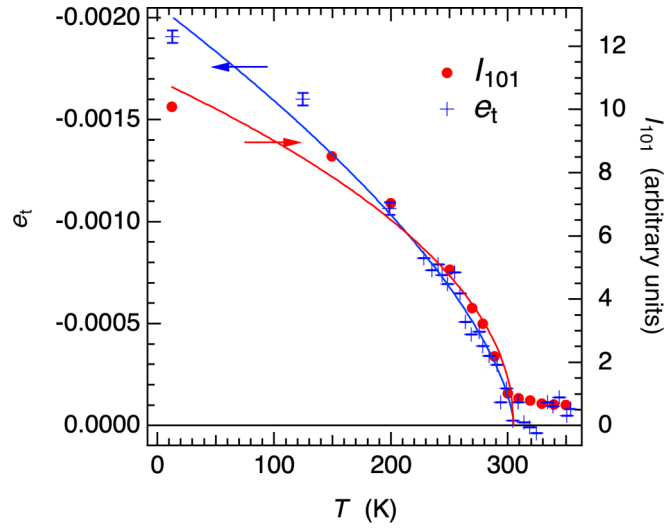

FIG. 1. Comparison of the variation of tetragonal shear strain, e_t, and the intensity of a magnetic ordering reflection, I_{101}, using raw data given in Azimonte *et al.* [16] for a sample of BFRO with 4% ± 1% Fe/Re disorder on B sites of the perovskite structure. Values of e_t at the three lowest temperatures were calculated using lattice parameters given by Ferreira *et al.* [17] from what appears to have been a sample prepared in the same way. Curves through the data are fits of the expression e_t (or I_{101}) $\propto A\,[(T_c - T)/T_c]^{2\beta}$ and have $\beta = 0.24 \pm 0.02$ for I_{101}, $\beta = 0.32 \pm 0.01$ for e_t, with $T_c = 305$ K. Although correlation between e_t and I_{101} seems only qualitative, disagreement between the fits is heavily dependent on two values for e_t at the lowest temperatures, which are not from the same data set as values at higher temperatures.

There are six strain components, e_1 to e_6, with e_a, e_t, and e_o in symmetry-adapted form as

$$e_a = e_1 + e_2 + e_3, \tag{2}$$

$$e_t = \frac{1}{\sqrt{3}}(2e_3 - e_1 - e_2), \tag{3}$$

$$e_o = e_1 - e_2. \tag{4}$$

Equilibrium conditions $\partial G/\partial e_t = \partial G/\partial e_a = 0$ give relationships between strains and the magnetic order parameter as

$$e_t = \frac{4\lambda_2 m_3^2}{\left(C_{11}^o - C_{12}^o\right)}, \tag{5}$$

$$e_a = \frac{-\lambda_1 m_3^2}{\frac{1}{3}\left(C_{12}^o + 2C_{12}^o\right)}. \tag{6}$$

The equilibrium condition $\partial G/\partial m_3 = 0$ (with $m_1 = m_2 = 0$) yields

$$m_3^2 = \frac{a(T_c - T)}{b^*}, \tag{7}$$

where

$$b^* = b + b' - \frac{2\lambda_1^2}{\frac{1}{3}\left(C_{11}^o + 2C_{12}^o\right)} + \frac{16\lambda_2^2}{\left(C_{11}^o - C_{12}^o\right)}. \tag{8}$$

The change in crystallographic space group is $Fm\bar{3}m \rightarrow I4/mmm$. If the transition was driven by some structural order

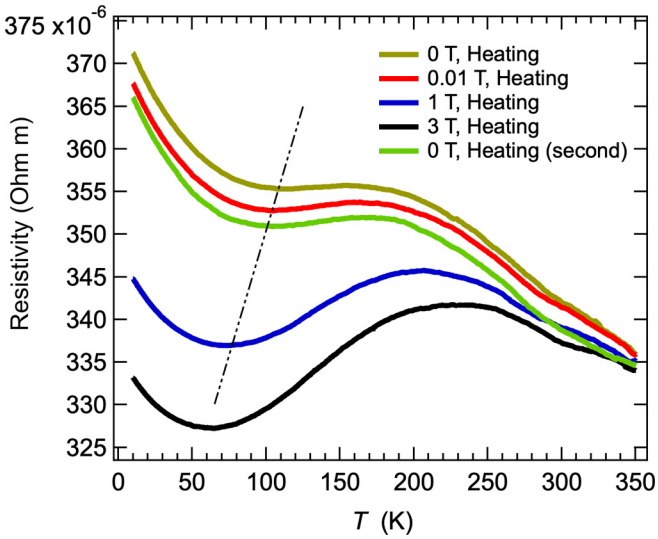

FIG. 2. Temperature and field dependences of the DC resistivity of a piece of ceramic sample 3. A dashed line marks the approximate locus of the temperature at which there is minimum in the resistivity with changing field. At lower field strengths it more nearly defines a saddle point. Data for the second heating sequence in zero field were collected after the measurements at progressively higher fields.

parameter, q, the transition would be pseudoproperly ferroelastic, $e_t \propto q$, because both e_t and q have the same symmetry (Γ_3^+). It would also be first order due to the presence in the Landau expansion of third-order terms in q, q^3. However, because the transition is driven by magnetic ordering, it is improperly ferroelastic [Eq. (5)] and can be continuous [Eq. (7)]. This model can be tested by comparing variations of tetragonal shear strain, e_t, and the intensity of a magnetic superlattice reflection, I_{101}, in neutron powder diffraction patterns, which is expected to scale with m_3^2.

Figure 1 shows a comparison of the temperature dependence of e_t and I_{101} from the literature. Values of linear strains are given by $e_1 = e_2 = (\sqrt{2}a–a_o)/a_o$, $e_3 = (c–a_o)/a_o$, where a, c are lattice parameters of the tetragonal structure and a_o is the lattice parameter of the cubic structure extrapolated below T_c. In the absence of a more complete set of lattice parameters, e_t has been determined from the strain data given in Fig. 2(a) of Azimonte *et al.* [16], assuming $a_o = a$ (without significant loss of precision). Values of e_t at the three lowest temperatures were calculated from lattice parameters given by Ferreira *et al.* [17], with a_o taken to be $(a^2c)^{1/3}$. The maximum value of $|e_t|$, ~0.002, is substantially smaller that the equivalent strain in SFMO, which includes octahedral tilting [8]. Values of the intensity of a magnetic ordering reflection in neutron powder diffraction patterns, I_{101}, were taken from Fig. 2(a) of Azimonte *et al.* [16]. Figure 1 shows, first, that both parameters vary continuously to zero at the transition point and, second, that there is some similarity between the temperature dependence of I_{101} with that of e_t. The data are perhaps permitting of improper ferroelastic behavior, $e_t \propto I_{101}(\propto m_3^2)$, but the correlation is not confirmed quantitatively, and more comprehensive data sets are needed for a definitive test of this.

III. SAMPLE PREPARATION AND CHARACTERIZATION

Polycrystalline Ba_2FeReO_6 (BFRO) samples were prepared by the standard solid-state route. A compound $Ba_2ReO_{5.5}$ was synthesized first by reaction of Re_2O_7 and $BaCO_3$ with a molar ratio of 1:4 at 1000 °C in air for 2 hr. Applying the corresponding balanced reaction, the $Ba_2ReO_{5.5}$ precursor was ground with Fe and Fe_2O_3 in a molar ratio of 6:4:1. The final powder was pressed uniaxially at 10 MPa to produce discs or cuboid pellets. The pellets were then heated in an evacuated sealed silica tube at 910 °C for 5 days, with a heating rate of 5 °C min^{-1}, and allowed to cool naturally. The final stage was to repeat the grinding and annealing procedure. Pressed pellets from the reground powder were annealed at 960 °C for 5 days. The heating rate was again 5 °C min^{-1}, and cooling was at the natural cooling rate of the furnace.

As set out in the Supplemental Material [21], the final product had the expected stoichiometry Ba_2FeReO_6, at least within rather wide experimental uncertainties. The degree of B/B′ disorder given by the proportion of antisite defects was ~5%. TEM-HAADF images and element maps of Ba, Fe, Re, and O confirmed a high degree of chemical homogeneity.

RUS measurements were made on pieces of two ceramic samples referred to below as sample 1 and sample 2. Sample 2 was the least friable of the ceramic disks prepared. Two pieces with approximate shapes of rectangular parallelepipeds were cut from it. Sample 2B had dimensions 1.005 × 3.786 × 3.623 mm^3 and mass 0.0832 g. Based on these parameters and a theoretical density calculated using the stoichiometric composition and cell dimension, the estimated porosity was ~20%. Sample 1 was friable, but an irregularly shaped piece with mass 0.101 g and approximate dimensions 5 × 5 × 1 mm^3 (sample 1A) gave well-resolved resonance peaks in RUS spectra collected at room temperature. Both samples 1A and 2B were free of any visible cracks.

RUS measurements above room temperature involved cycling up to ~600 K in air for periods of days. In order to check whether this treatment caused significant changes in chemistry or structure, the effects of heat treatment in air were tested separately with TGA/DSC and XPS. As shown in the Supplemental Material [21], the only change induced by heating powdered samples in air was a small weight loss, attributed to release of adsorbed moisture, and a small increase in oxygen content.

A separate ceramic pellet, referred to below as sample 3, was used for DC resistivity, DC magnetic, and AC magnetic measurements.

A. DC resistivity

Figure 2 shows the temperature dependence of DC resistivity, ρ, from a sintered polycrystalline ceramic sample in zero field and in fields of 0.01, 1, and 3 T. These data were collected in a Quantum Design Physical Properties Measurements System (PPMS) using the standard four-probe technique. The resistivity decreased with increasing temperature through two separate intervals, from ~10–100 K (0, 0.1 T) or ~10–60 K (1, 3 T) and ~200–350 K, with a plateau or maximum in between. A distinct minimum became more clearly defined

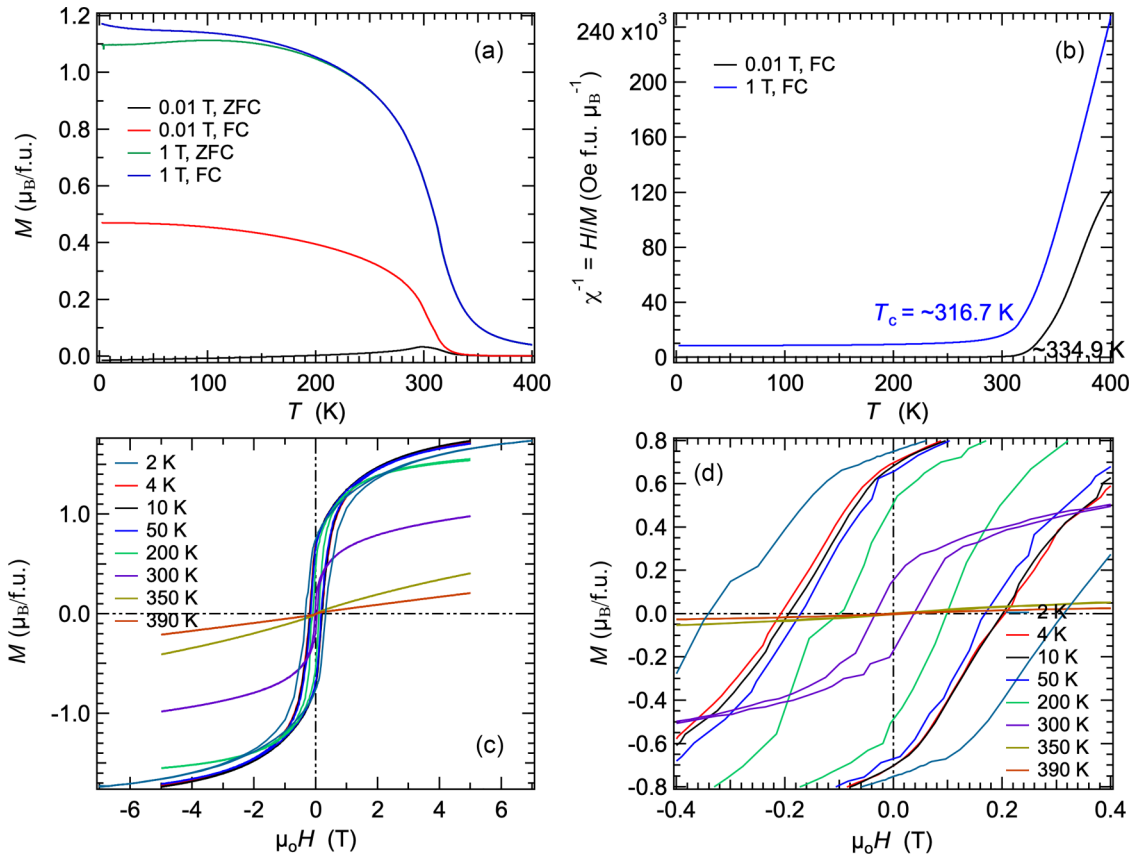

FIG. 3. (a) Thermal evolution of DC magnetization, M, of a piece of ceramic sample 3 with mass 0.022 g measured using fields of 0.01 T and 1 T under field-cooled (FC) and zero-field-cooled (ZFC) conditions. (b) Temperature dependence of inverse susceptibility, χ^{-1}. (c) Magnetization (M) vs magnetic field (H) curves collected at eight different temperatures between 2 and 390 K (d) Expanded view of the low field region in (c), showing open hysteresis loops at temperatures in the range 2–300 K, inclusive.

with increasing field, reducing to ~60 K in the 3 T field. At ~0.000327 Ω m, the observed values are higher than for a normal metal conductor, due to carrier scattering at grain boundaries, as widely observed for ceramic samples [22]. Application of a small magnetic field (0.01 T) slightly reduced the resistivity near room temperature, and further increases in the magnitude of the fields (1 T and 3 T) increased the magnitude of magnetoresistance (MR) at temperatures above 300 K. On remeasuring in zero field after measurements at high fields, the resistivity returned to the same pattern as observed at the start but with slightly lower values.

At temperatures below 200 K, the magnitude of MR increases remarkably with field. Defining the magnitude as

$$\mathrm{MR}(T,H) = [\rho(T,H=0)\ \rho(T,H)]/\rho(T,H) \qquad (9)$$

gave values of MR(300 K, 0.01 T) and MR(100 K, 0.01 T) as 0.2% and 0.8%, respectively. In a 3 T field, the values of MR(300 K, 3 T) and MR(100 K, 3 T) were 1.4%, 7.9%, respectively. For a half-metallic ferromagnet, this spin-dependent scattering normally occurs at grain boundaries or at magnetic domain boundaries [22].

B. DC magnetism

DC magnetic measurements were made in a Quantum Design PPMS measurement system. The temperature dependence of DC magnetization, M, through the temperature interval 4–395 K under field cooled (FC) and zero field cooled (ZFC) conditions from a piece of the ceramic sample is shown in Fig. 3(a). The evolution of M (FC) in 0.01 T indicates low-temperature saturation characteristic of spontaneous ferromagnetic ordering. The negative value of the M (ZFC) measured in 0.01 T could be due to the large coercivity, H_c, of a hard magnetic material [1]. A maximum magnetization was observed in the evolution of M (FC) at ~110 K in the 1 T data. Anomalous magnetization can be seen at ~67 K in the ZFC curve. Figure 3(b) shows paramagnetic evolution of the inverse susceptibility, χ^{-1}, between ~300 K and 395 K, for 0.01 T and 1 T, respectively. Solid red lines are fits for the Curie-Weiss expression, $\chi^{-1} = (T-\Theta)/C$, where C is the Curie constant and Θ is the Curie temperature, with C = ~5.1, Θ = ~334.9 K for 0.01 T, and C = ~3.4, Θ = ~316.7 K for 1 T.

M-H hysteresis loops measured in the range +5 to –5 T at seven temperatures between 4 and 390 K and in the range +7 to –7 T at 2 K are shown in Fig. 3(c). Saturation magnetization was not reached in the maximum applied field of 7 T at 2 K, consistent with results from other Re-based double perovskites where saturation magnetization is obtained only at fields >30 T due to the influence of magnetically disordered grain boundaries [23]. The low-temperature magnetization of the BFRO ceramic sample was ~1.74 μ_B fu^{-1} at

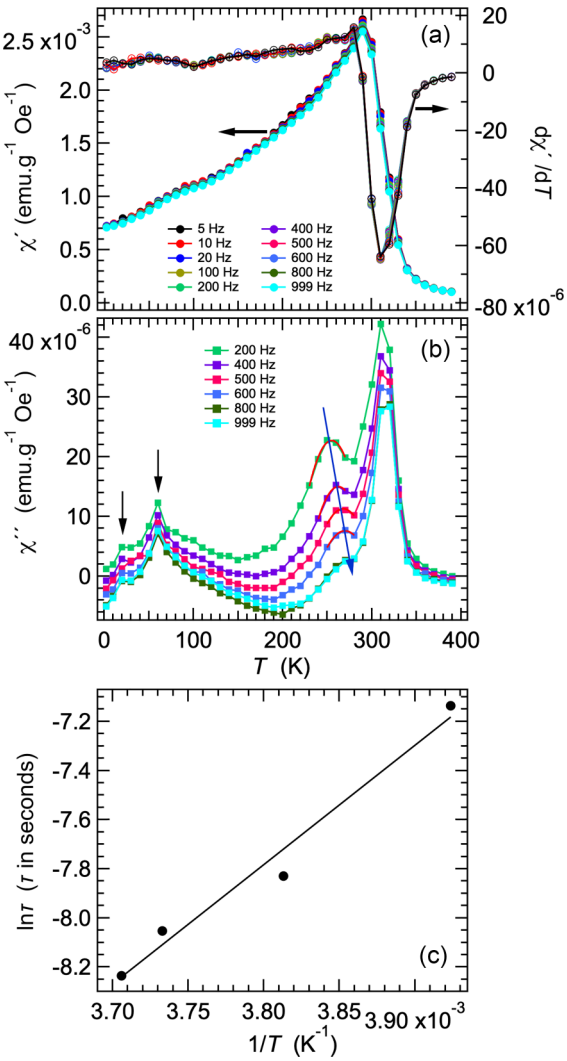

FIG. 4. AC magnetism data collected from a powdered sample of ceramic sample 3 with mass 0.07956 g. (a) The real component of susceptibility, χ', increased steeply falling temperature between ∼340 and ∼290 K, with a maximum in the gradient at ∼310 K. (b) The imaginary component, χ'', has four peaks. The temperature of peaks at ∼20, ∼60, and ∼310 K is independent of frequency, while the peak near 250 K has a marked temperature dependence. The amplitude of all four peaks decreased with increasing measuring frequency. (c) Arrhenius plot from fits to give the temperature, T_m, at which the frequency-dependent peaks in χ'' near 250 K had their maximum values. The straight line represents $\tau = \tau_o \exp(E_a/RT)$ with $\tau_o = 3.8 \times 10^{-12}$ s, $E_a = 0.42$ eV.

5 T, which is lower than the expected saturation value of 3.0 μ_B fu for antiparallel alignment of Fe^{3+}/Re^{5+} or Fe^{2+}/Re^{6+} spins. There are obvious loop openings between 2 and 300 K, typical of ferromagnetic behavior [Fig. 3(d)]. Both the remanent magnetization, $|M_r|$, and coercivity, $|H_c|$, increased with falling temperature. Their values at 2 K are ∼0.75 μ_B fu^{-1} and ∼0.34 T, respectively.

C. AC magnetism

AC magnetic data were collected using a Quantum Design magnetic property measurement system XL-7. Figure 4 shows the AC magnetic susceptibility of BFRO measured during heating from 2 K to 390 K of a powdered sample with mass 0.07956 g at frequencies of 5–999 Hz. The external DC field was 30 Oe, and the AC field amplitude was 1 Oe. The real component of the susceptibility, χ', increased steeply with falling temperature from low values at ∼390–350 K to a sharp maximum at ∼290 K, followed by steady decline. A maximum gradient of the steep rise between ∼340 and ∼290 K occurred at ∼310 K, corresponding to the expected magnetic transition point. The imaginary component, χ'', has four peaks [Fig. 4(b)]. The temperature of the peak at ∼310 K was independent of frequency, but the amplitude decreased systematically with increasing frequency. The position and amplitude of the smaller peak at ∼250 K varied with frequency, f, while only the amplitude of the peaks at ∼60 and ∼20 K were frequency dependent. Figure 4(c) is an Arrhenius plot for the frequency-dependent peak at ∼250 K, with τ as the relaxation time and T_{max} as the temperature at which a polynomial fit to the peak has its maximum value, corresponding to the condition $2\pi f\tau = 1$. The slope and intercept yielded an activation energy, E_a, of 0.42 $\pm$ 0.05 eV and $\ln \tau_o = -26.3 \pm 2.1$ ($\tau_o = 3.1 \times 10^{-11}$ to 4.6×10^{-13} s^{-1}) in $\tau = \tau_o \exp(E_a/RT)$.

IV. RESONANT ULTRASOUND SPECTROSCOPY

The RUS technique for investigating elastic and anelastic properties of millimeter-sized samples has been described by Migliori and Sarrao [24]. Details of the experimental protocols followed in the present study are given in Sec. S2 of the Supplemental Material [21] (see also references [25–27] therein). Two instruments were used in the present study. Spectra in the temperature range 3–309 K were collected in a helium atmosphere using an Oxford Instruments, cryogen-free Teslatron cryostat. Spectra through the temperature interval ∼290–600 K were collected in air.

Values of frequency, f, and peak width at half maximum height, Δf, for individual resonance peaks were obtained by fitting with an asymmetric Lorentzian function using the software package Igor (Wavemetrics). For a polycrystalline sample, variations of f^2 scale predominantly with the shear modulus, with only a minor influence of the bulk modulus due to much small contributions from breathing modes. Acoustic loss is expressed in terms of the inverse mechanical quality factor, Q^{-1}, which is taken to be $\Delta f/f$.

Estimates of the activation energy for loss mechanisms that give rise to peaks in the temperature dependence of Q^{-1} can be made using the expression [28–31]

$$Q^{-1}(T) = Q_m^{-1}\left\{\cosh\left[\frac{E_a}{Rr_2(\beta)}\left(\frac{1}{T} - \frac{1}{T_m}\right)\right]\right\}^{-1}. \quad (10)$$

R is the gas constant, Q_m^{-1} is the maximum loss at temperature T_m, E_a is an activation energy, and $r_2(\beta)$ is a width parameter which describes the spread of relaxation times. For a relaxation process with a single relaxation time, τ, the value of $r_2(\beta)$ is 1. $\omega\tau = 1$ at T_m, where $\omega = 2\pi f$, and $\tau = \tau_o \exp(E_a/RT)$ for a thermally activated process.

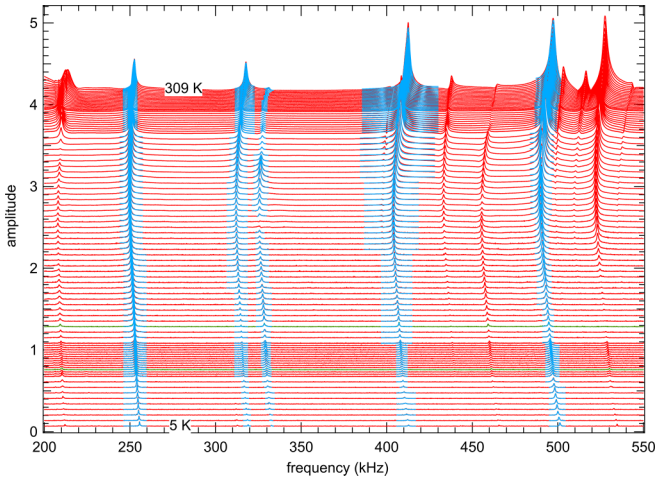

FIG. 5. Sample 2B. Segments of spectra in the frequency range ∼200–550 kHz, stacked up the y axis in proportion to the temperature at which they were collected during cooling. Blue curves are fits to selected resonance peaks.

For sample 2B, the sequence of measurements was low temperature first, followed by high temperatures. For sample 1A, the first measurements were made at high temperatures, followed by at low temperatures and then at high temperatures again.

A. Sample 2B

Figure 5 contains a stack of segments of spectra collected from sample 2B during cooling in the cryostat. All the resonance peaks showed slight softening with falling temperature followed by slight stiffening. Blue curves are fits to individual resonance peaks from which values of f and Δf were extracted. Figure 6(a) displays variations of f^2 and Q^{-1} from these, together with data for the heating sequence. Figure 6(b) contains data for one of the resonance peaks, as representative of the detailed variations.

The overall pattern of variations for f^2 values has a rounded minimum at ∼200 K, a slight increase in the rate of stiffening with falling temperature at ∼65 K and irreversibility between cooling and heating at $T >$ ∼100 K [Fig. 6(b)]. Q^{-1} data show weak peaks at ∼35 and ∼50 K, which correlate with the increasing slope in the temperature dependence

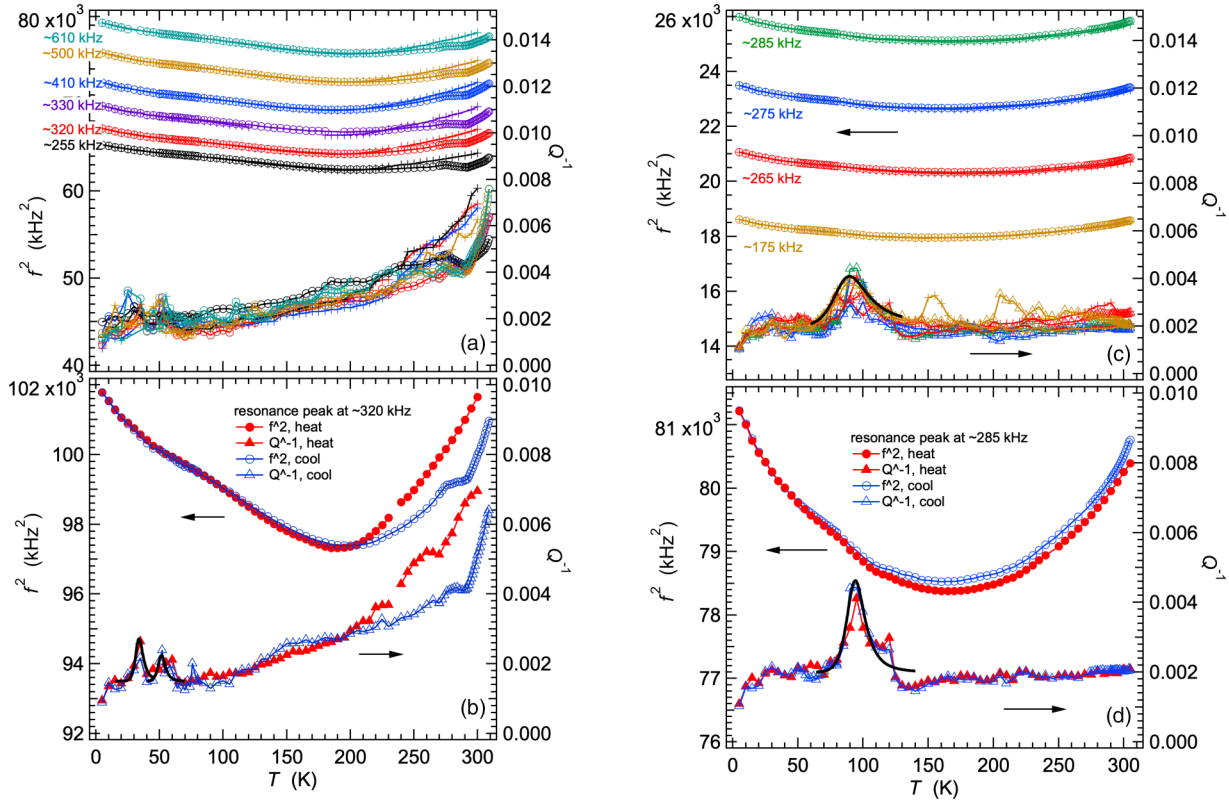

FIG. 6. (a), (b) Sample 2B. Variations in f^2 (left axis) and Q^{-1} (right axis) obtained from fits to individual resonance peaks in spectra collected throughout the full cooling (open circles)–heating (crosses) sequences below room temperature. Labels in kHz represent the approximate frequencies of the resonances concerned. Values of f^2 for each peak have been multiplied by arbitrary scaling factors in order to bring them closer together on the y axis, to allow easy comparison of their temperature dependences. The variations in f^2 (left axis) and Q^{-1} (right axis) for the resonance peak with frequency near 320 kHz are representative of some of the details. Black curves in (b) are fits of Eq. (10) to two peaks in Q^{-1}: $Q_m^{-1} = 0.0012 \pm 0.0002$, $E_a = 37 \pm 7$ meV, $T_m = 34 \pm 1$ K, $Q_m^{-1} = 0.0007 \pm 0.0002$, $E_a = 92 \pm 39$ meV, $T_m = 52 \pm 2$ K, for a constant baseline of 0.0015 and assuming $r_2(\beta) = 1$. (c), (d) Sample 1A. Equivalent variations of f^2 and Q^{-1} data for sample 1A, with the same labeling scheme. The black curves in (c) and (d) are fits of Eq. (10) with $Q_m^{-1} = 0.0021 \pm 0.0009$, $E_a = 59 \pm 3$ meV, $T_m = 90 \pm 1$ K, $Q_m^{-1} = 0.0026 \pm 0.0002$, $E_a = 125 \pm 13$ meV, $T_m = 94 \pm 1$ K, for a constant baseline of 0.002 and assuming $r_2(\beta) = 1$.

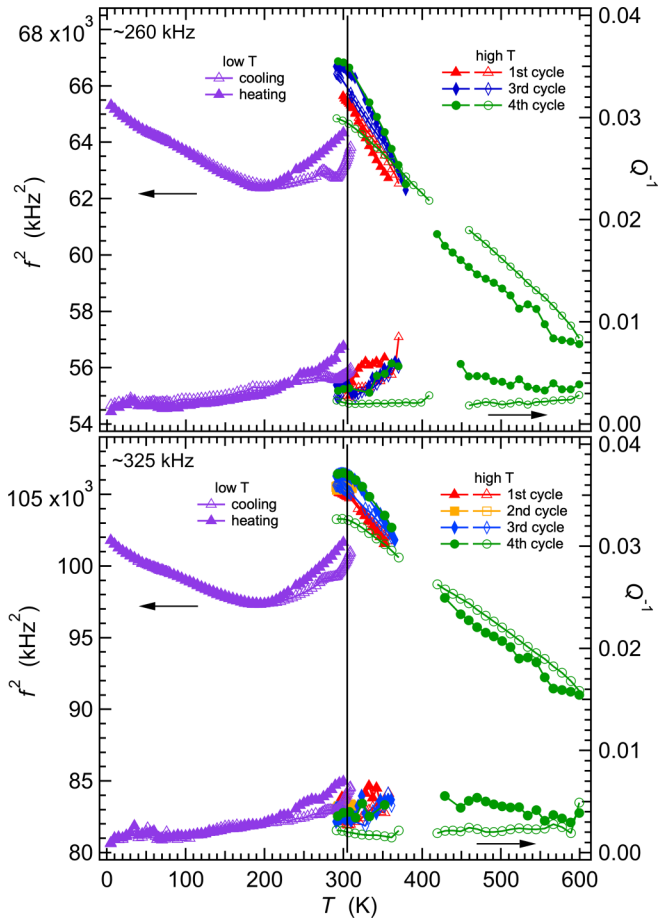

FIG. 7. Sample 2B. Variations of f^2 and Q^{-1} for four resonance peaks in spectra collected through the temperature interval 5–600 K. The frequency given for each data set is the approximate frequency of the relevant resonance. Filled symbols indicate heating and open symbols indicate cooling. The low-temperature cycle of cooling followed by heating was completed first. Four cycles of heating and cooling were then carried out above room temperature.

of f^2. They resemble the properties of classical Debye-like freezing processes with weak coupling to strain. Fits of Eq. (10) shown in Fig. 6(b) gave activation energies of ~40 and ~90 meV, respectively, assuming that each has a single relaxation time. These are minimum values if there is a spread of relaxation times. There is then an overall increase in Q^{-1} values with increasing temperature. Values of Q^{-1} between ~200 and ~300 K were lower during cooling than during heating, and the pattern of hysteresis between cooling and heating at temperatures above ~200 K correlates with the hysteresis seen in f^2. There are breaks in the slope of trends of both f^2 and Q^{-1} at ~292 and ~275 K in the cooling sequence which are absent from the heating sequence. The breaks in trend occur near, though not exactly coincidental with, changes in the effective cooling rate as the step size between data collections was increased from 1 to 2 K at 290 K and from 2 to 5 K at 270 K.

Figure 7 shows f^2 and Q^{-1} variations through the full temperature interval 5–600 K for two representative resonances with frequencies close to 260 and 325 kHz. The sequence of data collection was cooling and heating below room temperature followed by four cycles of heating and cooling above room temperature. Offsets in f^2 and Q^{-1} at room temperature between data collected in the high- and low-temperature instruments are at least partly experimental in origin. A contribution to the discontinuities arises because the signal at the sample has to pass through buffer rods in the high-temperature instrument rather than being transmitted directly to and from the transducers in the low-temperature instrument.

A maximum degree of softening, amounting to ~7%–9%, occurred between room temperature and ~200 K. Above room temperature the data show elastic softening with increasing temperature and approximately constant acoustic loss, a rounded maximum in f^2 values at ~300 K, and a degree of hysteresis between heating and cooling. The hysteresis between different heating/cooling cycles implies that details of the elastic properties at room temperature depend on the precise thermal history to which the sample had been subjected. In particular, the initial state before heating was elastically stiffer (higher values of f^2) and had higher acoustic loss (higher values of Q^{-1}) before heating to ~600 K than after cooling back to room temperature. Variations between cycles also occurred in response to heating to different maximum temperatures.

B. Sample 1A in zero field

Data for sample 1A from spectra collected in zero magnetic field are given in Figs. 6(c) and 6(d) and 8. High-temperature spectra were collected before transferring the sample to the cryostat, whereas spectra for sample 2B had been collected at low temperatures first.

The overall pattern of elastic softening/stiffening and acoustic loss in the temperature interval ~290–600 K for sample 1A is similar to that observed for sample 2B. A resonance with frequency near 280 kHz in spectra from sample 1A [Fig. 8(a)] illustrates some more specific features. Hysteresis between heating and cooling was greatest in the first cycle to ~600 K, with a reduction in f^2 by 10%. The f^2 values tended to drift upwards when the sample was sitting at room temperature between cycles. Q^{-1} values were also highest (0.008–0.012) in the first heating cycle and reverted to ~0.005 during cooling and in subsequent heating/cooling cycles. In more detail [Fig. 8(b)], a rounded maximum in values of f^2 occurred at ~300 K during heating. During cooling, small breaks in slope occurred when the temperature interval of data collection was reduced from ~9 K to ~1.5 K at ~335 K. The change to slower cooling rate resulted in the trend of f^2 shifting to slightly higher values.

Variations in f^2 and Q^{-1} values from spectra collected below room temperature for sample 1A are compared with values for sample 2B in Fig. 6. The broad pattern of softening with a rounded minimum, decreasing acoustic loss with falling temperature and hysteresis between cooling and heating is similar, but there are differences in detail. The differences are seen most clearly in the data for a single resonance [compare Figs. 6(b) and 6(d), for example]. Hysteresis in both f^2 and Q^{-1} values between heating and cooling of sample 1A started at ~50 K and became more evident above ~100 K. The magnitude of hysteresis effects was smaller in

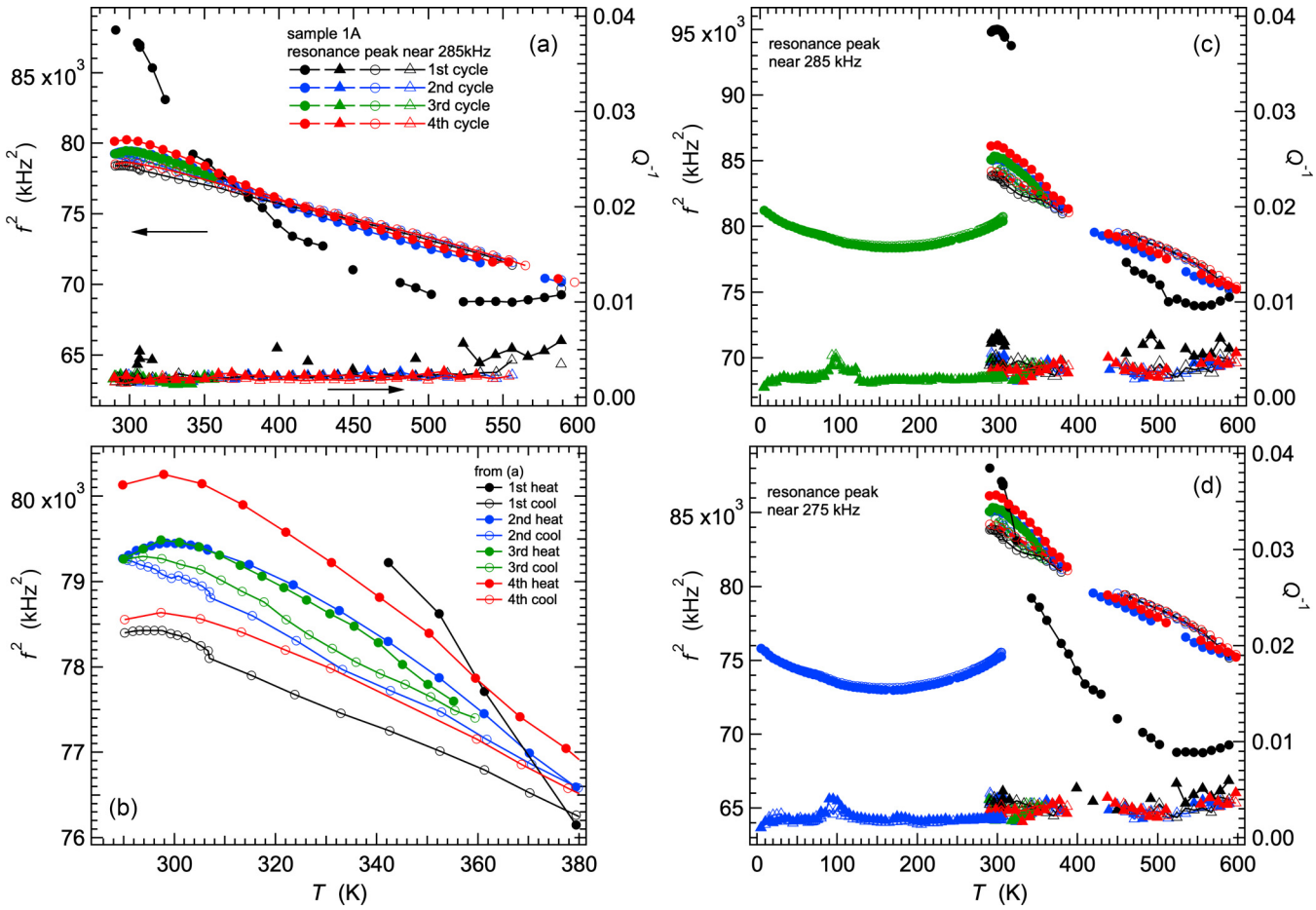

FIG. 8. Sample 1A. (a) Variations f^2 and Q^{-1} for a resonance peak with frequency near 280 kHz in spectra collected through successive heating/cooling cycles between ∼290 and ∼600 K. Filled circles = f^2 during heating, filled triangles = Q^{-1} during heating, open circles = f^2 during cooling, open triangles = Q^{-1} during cooling. Gaps in some sequences occur where the peak in the original spectrum was noisy or otherwise difficult to resolve. (b) Details from (a) of f^2 variations at and immediately above room temperature. The onset of softening with falling temperature occurred below ∼300 K, and there is a break in slope coinciding with a change in cooling rate at ∼306 K. (c), (d) Variations of f^2 and Q^{-1} across the full temperature interval, ∼5–600 K, for resonance peaks with frequencies near 285 and 275 K. As in Fig. 11, discontinuities in the data at room temperature are due, at least in part, to the change of instruments.

the case of 1A than 2B. Values of Q^{-1} for 1A are ∼0.002 between ∼130 and ∼300 K and increased only very slightly with increasing temperature, in contrast with the steeper increase seen in the data for 2B. For both samples, Q^{-1} values decrease markedly below ∼10 K. In place of the weak peaks in Q^{-1} near 35 and 50 K for sample 2B, there is one peak, or perhaps two overlapping peaks, near 100 K for sample 1A. Fits of Eq. (10) gave E_a ∼ 60 and ∼125 meV, assuming a single relaxation time for each loss process. Data for two resonance peaks covering the full experimental temperature interval ∼5–600 K show discontinuities at room temperature which are, again, attributable in part to the change between low- and high-temperature instruments. The magnitude of the discontinuity is larger for sample 1A than for sample 2B.

C. Sample 1A in applied magnetic field

Variations of f^2 and Q^{-1} from spectra collected from sample 1A with changing field between +2 and −2 T (0 → 2 → −2 → 0 T) at constant temperature are shown in two different ways in Fig. 9. Figure 9(a) contains data for a single resonance peak with frequency near 175 kHz at 4, 50, 100, 150, 200, 250, and 300 K. Other peaks showed the same pattern of stiffening with increasing and decreasing field from a rounded minimum at zero field when measured at 300, 250, and 200 K and a progressively more obvious double minimum from 150 down to 4 K. The total amount of stiffening at ±2 T, with respect to zero field, observed at 300 K was much less than at any of the other temperatures. Q^{-1} values were highest at 50 K.

Figures 9(b), 9(c), and 9(d) show variations of f^2 and Q^{-1} for a selection of resonances at 4, 200, and 300 K, respectively. Data from spectra collected at 50 K (not shown) resembled those collected at 4 K [Fig. 9(b)] though with a less pronounced double minimum. Data for 200 K [Fig. 9(c)] and 250 K (not shown) had a single rounded minimum with no obvious hysteresis with increasing and decreasing field. Slight differences in the steepness of the response of f^2 values from individual resonance to changing field must have arisen at least in part from their dependence on different combinations of the bulk and shear moduli. Q^{-1} values were very slightly higher in zero field, in comparison with ±2 T. Unlike the data for lower temperature, f^2 values collected at 300 K [Fig. 9(d)]

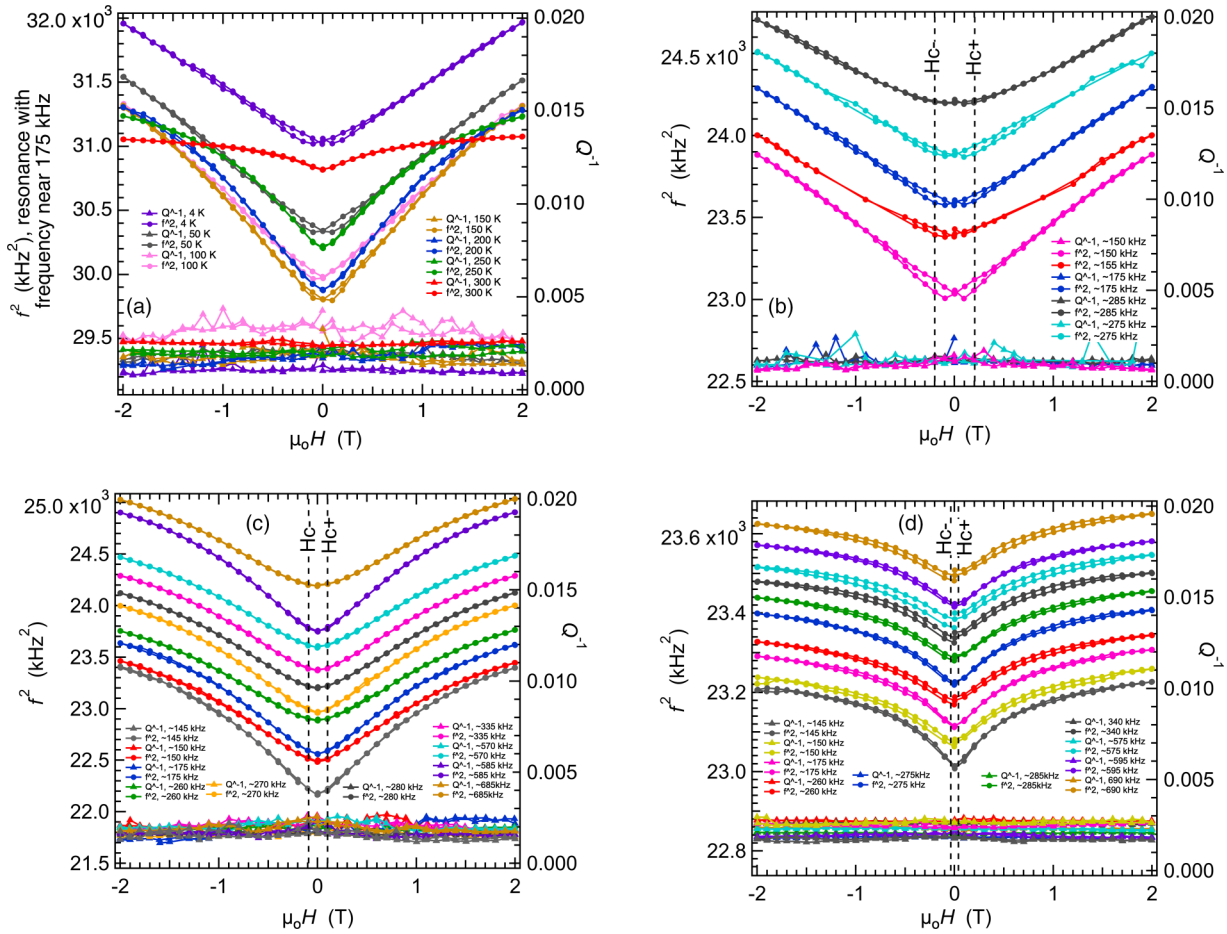

FIG. 9. Sample 1A. Variations of f^2 and Q^{-1} for selected resonance peaks in spectra collected with variable field, $0 \rightarrow +2 \rightarrow -2 \rightarrow 0$ T, at constant temperatures between 4 and 300 K. (a) Data for the resonance with frequency near 175 kHz at different temperatures, representative of variations shown by other resonances. At 4 K there is a double minimum in f^2 values which becomes a single minimum at higher temperatures. Q^{-1} values are highest at 50 K. (b) Data for resonances with different frequencies measured at 4 K. f^2 values have been shifted along the y axis with arbitrary scaling factors to allow comparison of different resonances. Data collected at 50 K (not shown) look generally similar, though with slightly less pronounced double minima. (c) Data for resonances with different frequencies measured at 200 K. A single rounded minimum is present for all resonances, without evidence of hysteresis between increasing and decreasing field. Data from spectra collected at 250 K (not shown) are similar. Values of Q^{-1} decrease slightly with increasing magnitude of the applied field. (d) Data for resonances with different frequencies measured at 300 K. There is a steady decrease in f^2 values throughout the fully sequence, with values at -2 T slightly lower than at $+2$ T. Vertical broken lines mark values of the coercive field, H_{c+} and H_{c-}, taken from the magnetic hysteresis loops shown in Fig. 3(d).

show a drift to progressively lower frequencies during the full sequence of changing field, $0 \rightarrow 2 \rightarrow -2 \rightarrow 0$ T. Also, unlike the data from lower temperature, f^2 values reached at $+2$ T were not the same as at -2 T.

Added to Figs. 9(b), 9(c), and 9(d) are values of coercive field for both directions of the applied field, H_{c+} and H_{c-}, taken from the magnetic hysteresis loops shown in Figs. 3(c) and 3(d).

Evolution of two specific features of the elastic properties is illustrated in more detail in Fig. 10. The resonance with frequency near 145 kHz at 4 K has a minimum above zero field during increasing field and the mirror image below zero during reducing field. This pattern is associated with relatively large values of coercive field, and the simplest explanation is that, at low fields, the initial effect of changing field relates mainly to poling of magnetic domains. On this basis, poled samples with more or less constant magnetization are slightly softer than samples with multiple magnetic domains.

Superimposed on a small effect from poling of the domains is a much large contribution of increasing magnetization by increasing alignment of individual moments parallel to the applied field. At 300 K [Fig. 10(b)], the coercivity is low and the main effect is increasing elastic stiffness with increasing magnitude of the field due to increasing induced magnetization. Superimposed on this, however, is an irreversible drift to lower f^2 values with time through the full sequence. This pattern is seen in f^2 results for most of the resonances shown in Fig. 9(d) but not for the resonance with lowest frequency, near 145 kHz. It is generally the case that the resonance with the lowest frequency is a pure shear mode, implying that the time-dependent, viscous component of the magnetic relaxation of the sample relates to the bulk modulus and, hence, to volume changes.

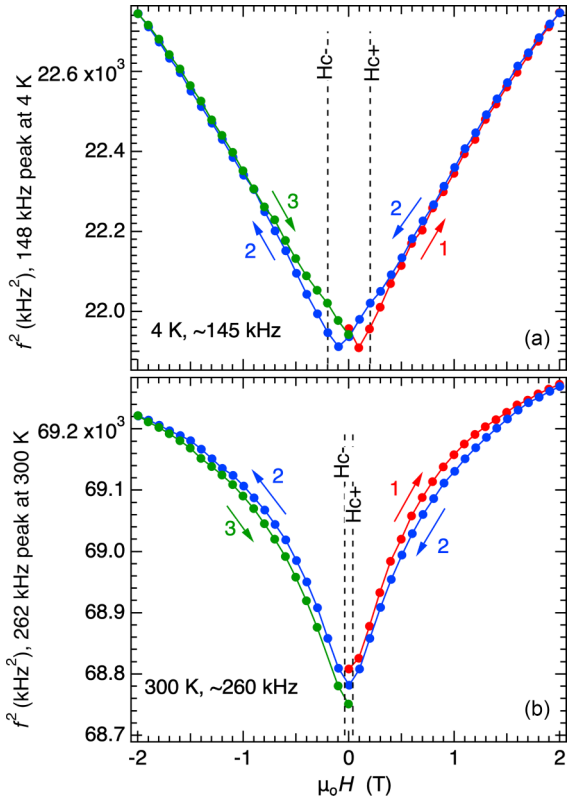

FIG. 10. Sample 1A. Details of f^2 variations with changing field at 4 K and 300 K: $0 \rightarrow +2$ T (1), $+2 \rightarrow -2$ T (2), -2 T $\rightarrow$ 0 T (3). (a) Within the limits of the coercive field at 4 K there is a double minimum, depending on the direction of change of applied field. This is attributed to poling of magnetic domains at low field strengths. (b) At 300 K there is a continuous, irreversible drift to lower values of f^2 with time during the full set of measurements.

f^2 and Q^{-1} data for nine resonances in spectra collected during a final heating stage from 3 to 303 K in a field of +2 T are shown in Fig. 11. f^2 variations show a different pattern with respect to heating in zero field, in that there are two breaks in the slopes for decreasing stiffness with increasing temperature. Each break in slope has an associated peak in Q^{-1} for which fits of Eq. (10) gave $T_m \sim 40$ K, $E_a \sim 20$ meV and $T_m \sim 100$ K, $E_a \sim 100$ meV, respectively, assuming a single relaxation time in each case. The temperature of the break in slope marked by a red dotted line at 51 K is independent of frequency, The second break in slope is not so well defined and increased from ~108 K at ~150 kHz to ~125 K at ~600 kHz.

D. Comparison with RUS results of Li *et al.* (2015)

RUS spectra presented by Li *et al.* [7] were collected in a single sweep through the temperature interval 50–375 K. They confirmed a smoothly rounded pattern of softening through the transition point, as opposed to the pattern of steep softening immediately below T_c typically seen for displacive transitions. Values of C_{44} and C_{11} in zero field and at 2 T were reported for a polycrystalline sample of BFRO which was assumed to be isotropic. Selected values of the bulk modulus, $K[= (1/3)(C_{11} + 2C_{12})]$, and shear modulus,

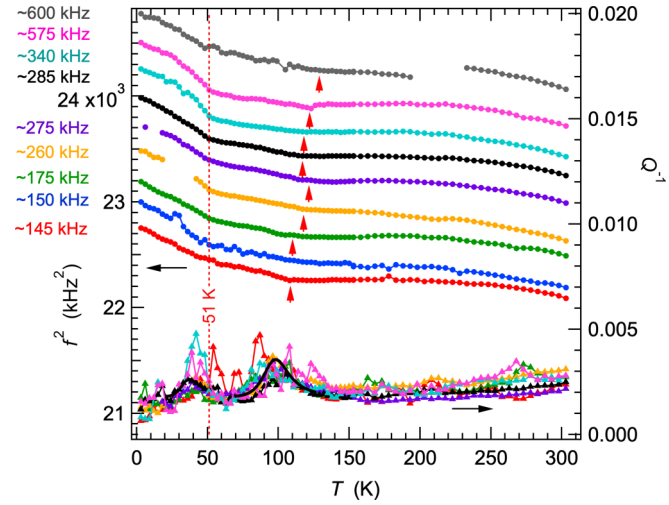

FIG. 11. Sample 1A: f^2 (filled circles) and Q^{-1} (filled triangles) for nine resonance peaks in spectra collected during heating from 3 to 303 K in a field of 2 T. f^2 values have been scaled arbitrarily along the y axis to allow easy comparison between the pattern of evolution of different resonances. A vertical dotted red line at 51 K marks the temperature at which a clear break in slope occurs in the temperature dependence of f^2 for all the resonances, independent of their frequencies. A second break in slope is marked by vertical red arrows but is less clear and appears to shift to higher temperatures with increasing frequency. Black curves are fits of Eq. (10) to two peaks in Q^{-1}: $Q_m^{-1} = 0.0008 \pm 0.0001$, $E_a = 20 \pm 3$ meV, $T_m = 37 \pm 1$ K, $Q_m^{-1} = 0.0018 \pm 0.0001$, $E_a = 105 \pm 11$ meV, $T_m = 98 \pm 1$ K, for a constant baseline of 0.0018 and assuming $r_2(\beta) = 1$.

$G[= C_{44} = (1/2)(C_{11} - C_{12})]$, extracted from these are compared with data obtained in the present study in Fig. 12.

Figure 12(a) contains a summary of RUS results from the present study alone for a resonance with frequency near 285 kHz. Since most resonances are dominated by shearing motions, the variations of f^2 are expected to scale with G. Minimum and maximum values of f^2 measured at constant temperature with varying field, i.e., at 0 and ± 2 T, are slightly lower and slightly higher, respectively, than the values obtained when measuring as a function of temperature at constant field, apart from at 4 K where there is a close match. Values of Q^{-1} from measurements as a function of temperature with variable field and as a function of field at constant temperature overlap with each other.

Li *et al.* [7] did not specify the density of their sample, and the stoichiometry might also have been different, but the overall forms of stiffening/softening as a function of temperature and of the effect of the 2 T field from the two studies are qualitatively the same [Fig. 12(b)]. The transition at ~310 K is marked by softening of the shear modulus with falling temperature, down to a minimum at ~175 K. This softening is substantially suppressed when the 2 T field is applied and the variation of the shear modulus becomes more nearly flat, with an increase below ~125 K. Differences in values of G between 0 and 2 T are compared with differences in f^2 for a resonance with frequency ~148 kHz in Fig. 12(c). Again, the pattern is the same, i.e., increasing differences down to ~175 K, followed by decreasing differences with falling

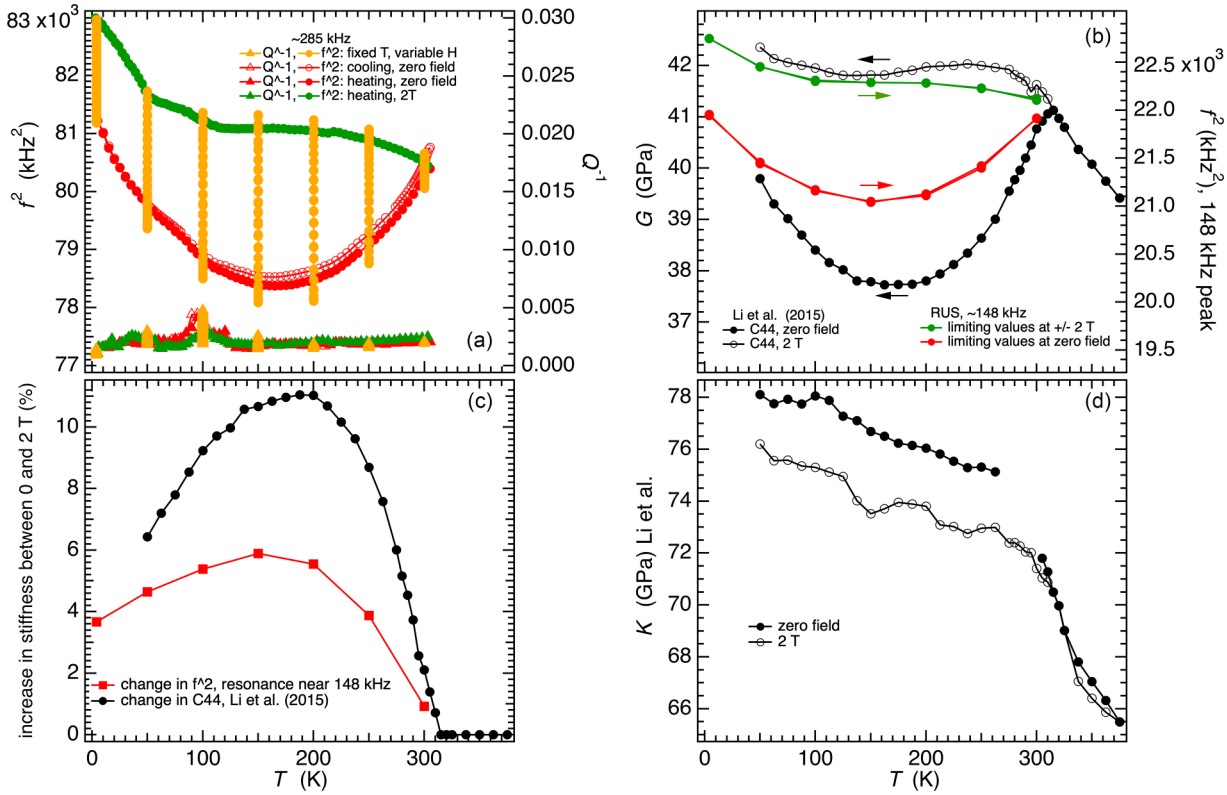

FIG. 12. Comparison of RUS data from the present study (sample 1A) with data for K and G calculated from selected values of C_{11} and C_{44} in Fig. 1 of Li *et al.* (2015). (a) Summary of f^2 and Q^{-1} data for a resonance with frequency near 285 kHz, from measurements made in the present study: red = zero field, varying temperature; green = 2 T field, varying temperature; orange = varying field at constant temperature. (b) Comparison of G (from data of Li *et al.*, black symbols, left axis) with f^2 for a resonance peak with frequency ∼148 kHz (this study, green and red symbols, right axis). The latter have been scaled so that they would coincide with the value of G at ∼310 K. (c) Differences between values of G or f^2 at zero field and 2 T, from (b). (d) Variation of K in zero field and in a 2 T field, as calculated from selected data in Fig. 1 of Li *et al.* [7].

temperature, though the magnitude of the change is smaller for the sample used in the present study. There are no data from the present study for the variation of K, but the data of Li *et al.* [7] show that the bulk modulus is softer at 2 T than in zero field, which is the opposite way around from G [Figs. 12(b) and 12(d)].

V. DISCUSSION

Softening of elastic moduli below the transition point of ferroelastic and coelastic transitions is a typical consequence of coupling between strain and the driving order parameter for a phase transition, as set out in many places in the literature [32–35]. In the case of an improper ferroelastic transition, the principal coupling term has the form $\lambda e_s q^2$, where λ is a coupling coefficient, e_s is the symmetry-breaking shear strain, and q is the driving order parameter. The mechanism is well understood and involves relaxation of the order parameter in response to an induced strain. A requirement for observation of the expected softening is that the relaxation time must be shorter than the timescale of the applied stress, i.e., $\sim 10^{-6}$ s for resonances with frequencies near 1 MHz.

Formal descriptions of changes in elastic moduli, C_{ik}, due to strain/order parameter coupling are derived from the function originally given by Slonczewski and Thomas [32]:

$$C_{ik} = C_{ik}^{o} - \sum_{l,m} \frac{\partial^2 G}{\partial e_i \partial q_l} . R_{lm} . \frac{\partial^2 G}{\partial e_k \partial q_m}, \tag{11}$$

where C_{ik}^{o} are elastic moduli without the influence of the phase transition and the second set of terms accounts for the effects of the transition. G is the excess free energy for the transition, e_i, e_k are strain components, and q_l, q_m are components of the order parameter. The matrix R_{lm} is the inverse of the matrix $\partial^2 G/\partial q_m \partial q_n$:

$$\sum_{m} R_{lm} . \frac{\partial^2 G}{\partial q_m \partial q_n} = \delta_{ln}. \tag{12}$$

The classic cases of $SrTiO_3$ [32,36] and $LaAlO_3$ [37] are representative of second-order transitions close to the displacive limit. Landau expansions with the form of Eq. (1) apply, and softening occurs abruptly through a narrow interval of only a few degrees below T_c. In BFRO, however, the softening occurs over an interval of ∼100 K below the transition point and recovers smoothly below a minimum at 150–200 K (Figs. 11 and 12 above, Fig. 1 of Li *et al.* [7]). This pattern must incorporate aspects of the different evolution of the second-order derivatives, $\partial^2 G/\partial q^2$, given that the exponent,

β, for the temperature dependence of the order parameter is ~0.23–0.3 (Fig. 1), rather than 0.5 for a second-order transition, and that the transition is likely to be close to the order/disorder limit rather than being displacive in character.

A further distinctive feature of the elastic properties of BFRO identified here is an overt sensitivity to the thermal history of the sample. Variations of f^2 above room temperature, in particular, differed between heating cycles. The evolution of sample 2B below room temperature also differed from that of sample 1A, which may have been due to the prior treatment to ~600 K of the latter. Hysteretic behavior between ~100 and ~600 K, together with changes in the trends in the temperature dependence of f^2 when heating or cooling rates were changed, points to significant kinetic control of the evolution of precursor microstructures and mixed magnetic/ferroelastic domains below the transition point. Equilibrium or, at least, fixed states were not achieved on timescales of hours/days at and immediately above room temperature.

Thus the overall pattern is, first, of softening of the shear modulus, indicative of classical strain/order parameter coupling with a thermodynamic potential determined by order/disorder behavior, and, second, of viscous relaxations which are most likely related to transformation microstructure(s). Individual factors in this picture are now considered in turn.

A. Stoichiometry and cation order

BFRO prepared for the present study had the perovskite structure and a high degree of B-site order, comparable with previous reports [14,15]. The composition was not tightly constrained by electron probe data, but equivalent checks of stoichiometry appear not to have been made in other studies. Standard practice seems to have been to assume that the nominal composition is correct, and it may be that a degree of nonstoichiometry is characteristic of different synthesis routes. The magnetic and elastic properties of the samples used here are comparable with those given in other reports. They showed the paramagnetic-ferrimagnetic transition at ~310 K, as expected from previous work [11–13]. In addition, DC magnetic properties shown in Fig. 2 are similar to those reported for the sample used for RUS measurements by Li *et al.* [7]. The form of softening shown for the shear modulus (given as C_{44}) in zero field and in a 2 T field by Li *et al.* [7] is also similar to data presented above for heating sequences. On the other hand, variations in stoichiometry could be responsible for differences in electrical transport properties. De Teresa *et al.* [13] and Fuoco *et al.* [15] reported DC resistivity values increasing with falling temperature, as found here, but Sleight and Weiher [11] and Prellier *et al.* [12] reported decreases.

B. Spin-orbit coupling

The rounded pattern of elastic softening behavior, without steep variations in Q^{-1}, falls between limiting cases of Sr_2FeMoO_6 (SFMO) on one hand and La_2FeMnO_6 (LFMO) or La_2NiMnO_6 (LNMO) on the other. The cubic ($Fm\bar{3}m$)-tetragonal ($I4/m$) transition in SFMO at ~420 K involves simultaneous magnetic and octahedral tilting transitions. RUS revealed a pattern of steep softening of the shear modulus by up to ~50%, with evidence of freezing/pinning of ferroelastic domain walls at ~340 K, typical of improper ferroelastics in which the principal strain coupling mechanism is with octahedral tilting [8].

Magnetic ordering transitions in LFMO and LNMO are not accompanied by changes in crystallographic space group and give rise to stiffening rather than softening of the shear modulus [9,10]. The paramagnetic-ferromagnetic transition at ~280 K in LNMO occurs in crystals which already have monoclinic ($P2_1/n$) or rhombohedral ($R\bar{3}c$) symmetry due to tilting transitions at much higher temperatures. It is not accompanied by spontaneous strains of sufficient magnitude to be detectable in currently available neutron diffraction data. Symmetry is also already broken at high temperatures by octahedral tilting in LFMO, and the structure at room temperature is in space group *Pnma*. The magnetic transition at ~280 K is to a cluster glass, but the only elastic anomalies appear to be Debye-like stiffening and acoustic loss at lower temperatures, interpreted as freezing of local ferromagnetic clusters.

The distinctive feature of BFRO, in comparison with these other double perovskites, is that the magnetic transition at ~310 K is accompanied by spin-orbit coupling [16–19,38]. This accounts for stronger coupling of the order parameter with strain, ferroelastic character, and the development of semimobile microstructures of domain walls or tweed which affect the bulk elastic properties. Relaxation of the order parameter in response to an applied stress in BFRO requires relaxation of both spins and the orbital order to which the spins are coupled, and the timescale is still sufficiently short that softening is observed at RUS frequencies. Pure spin effects, without coupled orbital effects in LFMO and LNMO, have a much weaker influence on both strain and elastic properties. The magnitude of the tetragonal shear strain will have been due predominantly to the orbital ordering, but values of e_t up to ~0.002 (Fig. 1) are still lower than those up to ~0.004 which accompany octahedral tilting in SFMO [8]. Given that the amount of softening is expected to scale with the square of the strain coupling term, λ, for coupling of the form $\lambda e_t q^2$, softening by up to ~10% in BFRO makes at least qualitative sense in comparison with ~50% softening in SFMO.

An additional observation of Li *et al.* [7] for BFRO was that the degree of softening reduced progressively when RUS measurements were made with the ceramic sample held in magnetic fields of 0.5, 1, and 2 T. For explanation they referred to the analogous effect of magnetic field on the Young's modulus of polycrystalline nickel described by Siegel and Quimby [39]. The field imposes preferred orientations of magnetic moments and reduces the contribution of magnetoelastic relaxations arising from an imposed stress. This is equivalent to reducing the amount of softening that could occur by the classical mechanism implied by Eq. (1). In more formal terms, the effect of the field is to reduce the value of the second-order derivatives of free energy with respect to the degree of order, R_{lm}. At the limit of all individual spin moments held in parallel alignment by a strong external field, dynamic stress of low magnitude would induce a shear strain but would not result in an additional relaxation of the spins. If higher order strain coupling terms such as $\lambda e^2 q^2$ are small, the measured elastic moduli will be C_{ik}^{o} in Eqs. (1) and (11).

In contrast, the bulk modulus calculated from values of C_{11} and C_{44} of Li *et al.* [7] shows softening by ∼2.5%, rather than stiffening, as the consequence of applying a 2 T field [Fig. 12(d)]. No experimental uncertainties were given with the original data, so this could be an artifact, but, if the effect is real, one possible explanation is that the change is related to an increase in volume associated with alignment of all individual moments in the field. Figures S2(c) and S2(d) [21] provide a hint that the volume strain, e_a, coupled with the magnetic order parameter is positive, consistent with a magnetically ordered sample having a larger molar volume than a disordered sample. These issues are not resolved here.

C. Microstructure dynamics: Precursor effects

Variations of the elastic moduli of a homogeneous crystal arising from a classical strain relaxation mechanism should be fully reversible for a thermodynamically continuous transition, whereas there is a distinct hysteresis in the evolution of both f^2 and Q^{-1} between heating and cooling in the interval ∼200–300 K for BFRO (Figs. 6 and 7). Hysteretic effects seen both above and below the transition point are consistent with the presence of microstructures that depend on the thermal history of the sample and can evolve on a timescale of hours and days at room temperature. For example, variations in the evolution of f^2 occurred when the cooling rate changed at temperatures between ∼270 and ∼310 K (Figs. 6–8). Above the transition point, the microstructure presumably contained clusters with locally aligned spin moments, orbital order, and shear strain.

Expected microstructures are a weak precursor tweed pattern or clusters analogous to polar nanoregions in relaxor ferroelectrics. Variations in the dimensions and configurations of these would influence the degrees of local order and local strain, contributing to variations of the elastic properties.

The largest variations in shear modulus, scaling with f^2, and the highest acoustic loss, scaling with Q^{-1}, occurred in the first heating sequence of sample 1A (Fig. 8), indicating that the structural state of the initial sample was significantly different after it had been heated up to ∼600 K. There may be some contribution from a slight increase in oxygen content, identified by XPS (Sec. S1.5 of the Supplemental Material [21]), but it is more likely that a pattern of tetragonal domains developing during weeks and months at room temperature does not return in a period of hours/days following cycling through the transition point.

In the vicinity of T_c, ferroelastic twins are expected to develop initially in the form of a tweed microstructure. A more or less static microstructure at room temperature, developing by conversion from a precursor state through to discrete ferroelastic domain walls, would then cause the observed rounding of the shear modulus through T_c.

D. Microstructure dynamics: Pinning/freezing of ferroelastic twin walls

Purely ferroelastic twin walls are expected to have widths on the order of a few unit cells [40], while magnetic domain walls are likely to be ∼10–100 times wider, depending on the degree of magnetic anisotropy. We find that 90º magnetic domain walls will also be ferroelastic, while 180º walls will not. It follows that ferroelastic domain walls in BFRO can contain gradients of both shear strain and ferrimagnetic moment. Coupling between the two gradients should play a significant role in determining the widths of the walls which develop and will be important also in controlling the development of tweed, as opposed to a microstructure of discrete domain walls. It will also determine their interaction with defects in the underlying crystal structures and, hence, control their mobility in response to an applied stress.

For a displacive transition with second-order character the width, w, and density, N, of ferroelastic domain walls are expected to vary according to $w \propto N \propto (T_c - T)^{-1}$ [40–43], with the result that the distinction between domains and domain walls becomes diffuse close to T_c. In the cases of $LaAlO_3$ and $SrTiO_3$, the twin walls give rise to high acoustic loss in RUS measurements because segments of them can move on a timescale of faster than $\sim 10^{-5}$–10^{-6} s in response to an applied shear stress [29,44,45]. No increase in acoustic loss has been seen below T_c of BFRO, but this does not necessarily mean that all domain walls were fully pinned.

The temperature of the peak in χ'' at the transition point from AC magnetic measurements at frequencies of 0.2–1 kHz (Fig. 4) is independent of frequency and is therefore most likely related to critical slowing down of dynamic flipping of magnetic moments. The same effect is not seen in data for Q^{-1}, implying that any strain relaxation associated with these spin oscillations is slower than $\sim 10^{-5}$ to 10^{-6} s. However, the AC magnetic data show a frequency-dependent magnetic peak in $\chi'' \sim$ 20–50 K below T_c [Fig. 8(b)]. Treating this as arising from a thermally activated loss process yielded an activation energy of ∼0.42 eV and a relaxation time, τ_o, of $\sim 4 \times 10^{-12}$ s [Fig. 8(c)]. By extrapolation, the magnetic loss peak would shift to ∼380 K if measured at 100 kHz. This is above T_c for BFRO but is not far from the acoustic loss peak seen at ∼340 K in RUS data from SFMO, for which E_a was estimated to be ∼0.65 eV (Yang *et al.* 2016 PRB 93 024101) [8].

The activation energy for pinning of ferroelastic twin walls by oxygen vacancies in oxide perovskites is characteristically ∼0.91.1 eV [46], while lower values have been observed for the domain wall freezing process in $BiFeO_3$ (∼0.6 eV [47]) and in $KMnF_3$ (∼0.13–0.42 eV [31,48,49]). The comparison with SFMO, in particular, allows interpretation of the magnetic loss peak from BFRO as being due to freezing of ferromagnetic + ferroelastic domain walls that are mobile immediately below ∼310 K when measured with a dynamic external field at $\sim 10^2$–10^3 Hz but immobile when measured at $\sim 10^5$–10^6 Hz.

Small difference in f^2 values observed between cooling and heating in the temperature interval ∼100–300 K can be understood in terms of the evolution of the ferroelastic domain structure if the domain walls are still able to evolve to some degree during cooling on a timescale of hours/days. The obvious evolution would be by (irreversible) domain coarsening or by interaction with grain boundaries. Any changes in the overall proportions of twin domains in different orientations throughout the polycrystalline sample that developed could lead to small increases or small decreases in the shear modulus of the bulk sample, depending

on the exact changes in domain configuration. In the case of sample 2B, f^2 values were higher after cycling down to the lowest temperatures while for sample 1A they were lower (Fig. 6).

E. Magnetoelastic relaxation processes at $T < 100$ K

BFRO must contain abundant local heterogeneities which could contribute to the magnetoelastic relaxation behavior at the lowest temperatures. These include grain boundaries, some degree of B-site cation disorder (antisite defects), some proportion of vacancies, microstructures consisting of ferroelastic domain walls, and boundaries between antiphase domains arising from the symmetry change driven by ordering of B-site cations. Antiphase boundaries arising from cation ordering are known to accommodate antisite defects and to have a significant influence on the magnetic properties of SFMO and Ba_2FeMoO_6, for example [50–55]. The presence of frequency-dependent and frequency-independent peaks in χ'' appears to be characteristic of other magnetic double perovskites such as LNMO and LFMO [7,10,56–58]. The peak in Q^{-1} and change of slope in f^2 at ∼95 K in Figs. 6(c) and 6(d) mark the temperature below which no further hysteresis of f^2 values occurred in zero field. They also mark the temperature below which a double minimum in f^2 appeared when the field was varied at constant temperature [Fig. 9(a)]. If the interpretation of hysteretic effects given above is correct, this is due to freezing of remaining segments of magnetic/ferroelastic domain walls that had remained mobile to any extent.

Fitting of additional peaks in Q^{-1} at ∼34 K and ∼52 K in Fig. 6(b) (zero field) gave ∼37 and ∼92 meV, and ∼20 meV for the peak at 37 K in Fig. 11 (2 T field), assuming a single relaxation time in each case. Using the measuring frequency as ∼320 kHz yields an estimate of τ_o as $\sim 10^{-12}$ and $\sim 10^{-15}$ s, for the first two and ∼285 kHz for the third gives $\tau_o \sim 10^{-9}$ s. Loss peaks observed at similar temperatures in other perovskites have also yielded activation energies in the range ∼30–70 meV ($GdMnO_3$, $TbMnO_3$, and $Sm_{0.6}Y_{0.4}SmO_3$ [10,28,59]. These all overlap with values in the range ∼40–80 meV from dielectric spectroscopy measurements, which are characteristic of pinning/freezing of polarons in perovskites [60], which could also be a contributing factor to the increase in DC resistivity of BFRO seen below ∼100 K in zero field and below ∼60 K in a 3 T field (Fig. 2).

Peaks in χ'' at ∼60 and ∼20 K [Fig. 4(b)] indicate the existence of magnetic loss processes, and it seems likely that the strain relaxations and magnetic relaxations are related. However, the peaks in χ'' did not shift in temperature with changing frequency, as would be expected for magnetic phase transitions rather than for thermally activated Debye-like freezing processes. While there is a break in slope at ∼75 K of the ZFC magnetization measured in a 1 T field [Fig. 3(a)], there is as yet no convincing evidence for additional magnetic phase transitions at these low temperatures.

VI. CONCLUSIONS

Spin-orbit coupling is effectively synonymous with spin-lattice coupling if the spontaneous strain arises essentially as a consequence of changes in electronic structure that are strongly dependent on spin state. In the case of the ferrimagnetic/ferroelastic transition in BFRO, the relaxation time of spins in response to a small induced dynamic strain at ∼0.1–1 MHz is sufficiently fast that softening of the shear modulus can occur. However, ferroelastic domain walls appear to be immobile on this timescale, and it is proposed that a microstructure which evolves in a viscous manner on a timescale of hours/days develops both above and below the transition point.

The observed elastic and anelastic properties highlight subtle differences in the magnetoelastic coupling behavior of Ba_2FeReO_6 in comparison with other double perovskites such as Sr_2FeMoO_6, La_2NiMnO_6, and La_2FeMnO_6. Key variables between these phases are, first, the presence or absence of tilting transitions and different degrees of B-site order. Such constraints must also have implications for the structure and properties of domain walls and the presence of local heterogeneities in double perovskites more widely.

Ferroelastic domain walls in BFRO must contain gradients of ferrimagnetic moments, 180° magnetic domain walls are expected to be free of shear strains, and antiphase domains due to B-site ordering give rise to local anomalies in magnetic structure. The result is a material with abundant heterogeneities coupled with strain on different length scales which could be tuned by choice of composition, thermal history, and cation order.

ACKNOWLEDGMENTS

This work was supported financially by the National Science Fund for Distinguished Young Scholars (52225312), the Fundamental Research Funds for the Provincial Universities of Zhejiang (No. GK229909299001-002), the Open Foundation of the State Key Laboratory of Modern Optical Instrumentation (MOI2022-1), the National Natural Science Foundation of China (Grants No. 51702289 and No. U1908220), and the Zhejiang Provincial Key Research and Development Program (2021C01033). RUS facilities in Cambridge were established through grants from the Natural Environment Research Council (Grants No. NE/B505738/1 and No. NE/F017081/1) and the Engineering and Physical Sciences Research Council (Grant No. EP/I036079/1) to M.A.C.

[1] D. Serrate, J. M. De Teresa, and M. R. Ibarra, Double perovskites with ferromagnetism above room temperature, J. Phys.: Condens. Matter **19**, 023201 (2007).

[2] M. P. Singh, K. D. Truong, S. Jandl, and P. Fournier, Multiferroic double perovskites: Opportunities, issues, and challenges, J. Appl. Phys. **107**, 09D917 (2010).

[3] Y. Shimakawa, M. Azuma, and N. Ichikawa, Multiferroic compounds with double-perovskite structures, Materials **4**, 153 (2011).

[4] S. Vasala and M. Karppinen, $A_2B'B''O_6$ perovskites: A review, Progr. Solid State Chem. **43**, 1 (2015).

[5] T. Jia, Z. Zeng, and H. Q. Lin, The collinear ↑↑↓↓ magnetism driven ferroelectricity in double-perovskite multiferroics, J. Phys.: Conf. Ser. **827**, 012005 (2017).

[6] G. Catalan, J. Seidel, R. Ramesh, and J. F. Scott, Domain wall nanoelectronics, Rev. Mod. Phys. **84**, 119 (2012).

[7] L. Li, M. R. Koehler, I. Bredeson, J. He, D. Mandrus, and V. Keppens, Magnetoelastic coupling in A_2FeReO_6 (A = Ba and Ca) probed by elastic constants and magnetostriction measurements, J. Appl. Phys. **117**, 213913 (2015).

[8] D. Yang, R. J. Harrison, J. A. Schiemer, G. I. Lampronti, X. Liu, F. Zhang, H. Ding, Y. Liu, and M. A. Carpenter, Magnetostructural coupling behavior at the ferromagnetic transition in double-perovskite Sr_2FeMoO_6, Phys. Rev. B **93**, 024101 (2016).

[9] D. Yang, G. I. Lampronti, C. R. Sebastian Haines, and M. A. Carpenter, Magnetoelastic coupling behavior at the ferromagnetic transition in the partially disordered double perovskite La_2NiMnO_6, Phys. Rev. B **100**, 014304 (2019).

[10] D. Yang, T. Yang, P. Mukherjee, S. E. Dutton, D. Huo, and M. A. Carpenter, Strain coupling and acoustic attenuation associated with glassy magnetic phase transitions in the disordered double perovskite La_2FeMnO_6, Phys. Rev. B **99**, 094314 (2019).

[11] A. W. Sleight and J. F. Weiher, Magnetic and electrical properties of Ba_2MReO_6 ordered perovskites, J. Phys. Chem. Sol. **33**, 679 (1972).

[12] W. Prellier, V. Smolyaninova, A. Biswas, C. Galley, R. L. Greene, K. Ramesha, and J. Gopalakrishnan, Properties of the ferrimagnetic double perovskites A_2FeReO_6 (A = Ba and Ca), J. Phys.: Condens. Matter **12**, 965 (2000).

[13] J. M. De Teresa, D. Serrate, J. Blasco, M. R. Ibarra, and L. Morellon, Impact of cation size on magnetic properties of $(AA')_2\,Fe\,Re\,O_6$ double perovskites, Phys. Rev. B **69**, 144401 (2004).

[14] J. Gopalakrishnan, A. Chattopadhyay, S. B. Ogale, T. Venkatesan, R. L. Greene, A. J. Millis, K. Ramesha, B. Hannoyer, and G. Marest, Metallic and nonmetallic double perovskites: A case study of A_2FeReO_6 (A = Ca, Sr, Ba), Phys. Rev. B **62**, 9538 (2000).

[15] L. Fuoco, D. Rodriguez, T. Peppel, and P. A. Maggard, Molten-salt-mediated syntheses of Sr_2FeReO_6, Ba_2FeReO_6, and Sr_2CrReO_6: Particle sizes, B/B′ site disorder, and magnetic properties, Chem. Mater. **23**, 5409 (2011).

[16] C. Azimonte, J. C. Cezar, E. Granado, Q. Huang, J. W. Lynn, J. C. P. Campoy, J. Gopalakrishnan, and K. Ramesha, Incipient Orbital Order in Half-Metallic Ba_2FeReO_6, Phys. Rev. Lett. **98**, 017204 (2007).

[17] F. F. Ferreira, E. Granado, W. Carvalho, Jr., S. W. Kycia, D. Bruno, and R. Droppa, Jr., X-ray powder diffraction beamline at D10B of LNLS: Application to the Ba_2FeReO_6 double perovskite, J. Synchrotron Radiat. **13**, 46 (2006).

[18] K. W. Plumb, A. M. Cook, J. P. Clancy, A. I. Kolesnikov, B. C. Jeon, T. W. Noh, A. Paramekanti, and Y.-J. Kim, Neutron scattering study of magnetic excitations in a 5d-based double-perovskite Ba_2FeReO_6, Phys. Rev. B **87**, 184412 (2013).

[19] A. Cook and A. Paramekanti, Theory of metallic double perovskites with spin-orbit coupling and strong correlations: Application to ferrimagnetic Ba_2FeReO_6, Phys. Rev. B **88**, 235102 (2013).

[20] H. T. Stokes, D. M. Hatch, and B. J. Campbell, ISOTROPY Software Suite, https://iso.byu.edu/iso/isotropy.php.

[21] See Supplemental Material at http://link.aps.org/supplemental/10.1103/PhysRevB.107.144108 for details of characterization of the sample by x-ray diffraction, including *in situ* at high temperatures, transmission electron microscopy, and electron probe microanalysis. Data are presented showing the effect of heating the sample in air on weight loss and oxygen content, and experimental details of the RUS measurements are described. The material also contains Refs. [25–27].

[22] K.-I. Kobayashi, T. Kimura, H. Sawada, K. Terakura, and Y. Tokura, Room-temperature magnetoresistance in an oxide material with an ordered double-perovskite structure, Nature (London) **395**, 677 (1998).

[23] J. M. Michalik, J. M. De Theresa, J. Blasco, P. A. Algarabel, M. R. Ibarra, Cz. Kapusta, and U. Zeitler, Temperature dependence of magnetization under high fields in Re-based double perovskites, J. Phys.: Condens. Matter **19**, 506206 (2007).

[24] A. Migliori and J. L. Sarrao, *Resonant Ultrasound Spectroscopy: Applications to Physics, Material Measurements, and Nondestructive Evaluation* (Wiley, New York, 1997).

[25] J. Schiemer, L. J. Spalek, S. S. Saxena, C. Panagopoulos, T. Katsufuji, A. Bussmann-Holder, J. Köhler, and M. A. Carpenter, Magnetic field and in situ stress dependence of elastic behavior in $EuTiO_3$ from resonant ultrasound spectroscopy, Phys. Rev. B **93**, 054108 (2016).

[26] D. M. Evans, J. A. Schiemer, M. Schmidt, H. Wilhelm, and M. A. Carpenter, Defect dynamics and strain coupling to magnetization in the cubic helimagnet Cu_2OSeO_3, Phys. Rev. B **95**, 094426 (2017).

[27] R. E. A. McKnight, C. J. Howard, and M. A. Carpenter, Elastic anomalies associated with transformation sequences in perovskites: I. Strontium zirconate, $SrZrO_3$, J. Phys.: Condens. Matter **21**, 015901 (2008).

[28] M. A. Carpenter, C. J. Howard, R. E. A. McKnight, A. Migliori, J. B. Betts, and V. R. Fanelli, Elastic and anelastic relaxations associated with the incommensurate structure of $Pr_{0.48}Ca_{0.52}MnO_3$, Phys. Rev. B **82**, 134123 (2010).

[29] M. A. Carpenter and Z. Zhang, Anelasticity maps for acoustic dissipation associated with phase transitions in minerals, Geophys. J. Int. **186**, 279 (2011).

[30] M. Weller, G. Y. Li, J. X. Zhang, T. S. Ke, and J. Diehl, Accurate determination of activation enthalpies associated with the stress-induced migration of oxygen or nitrogen in tantalum and niobium, Acta Metall. **29**, 1047 (1981).

[31] M. A. Carpenter, E. K. H. Salje, and C. J. Howard, Magnetoelastic coupling and multiferroic ferroelastic/magnetic phase transitions in the perovskite $KMnF_3$, Phys. Rev. B **85**, 224430 (2012).

[32] J. C. Slonczewski and H. Thomas, Interaction of elastic strain with the structural transition of strontium titanate, Phys. Rev. B **1**, 3599 (1970).

[33] W. Rehwald, The study of structural phase transitions by means of ultrasonic experiments, Adv. Phys. **22**, 721 (1973).

[34] B. Lüthi and W. Rehwald, Ultrasonic studies near structural phase transitions, in *Structural Phase Transitions I* edited by K. A. Müller and H. Thomas (Springer, Berlin, 1981), p. 131.

[35] M. A. Carpenter and E. K. H. Salje, Elastic anomalies in minerals due to structural phase transitions, Eur. J. Mineral. **10**, 693 (1998).

[36] M. A. Carpenter, Elastic anomalies accompanying phase transitions in (Ca,Sr)TiO_3 perovskites: Part I. Landau theory and a calibration for $SrTiO_3$, Am. Mineral. **92**, 309 (2007).

[37] M. A. Carpenter, S. V. Sinogeikin, J. D. Bass, D. L. Lakshtanov, and S. D. Jacobsen, Elastic relaxations associated with the *Pm*-3*m*–*R*-3*c* transition in $LaAlO_3$: I. Single crystal elastic moduli at room temperature, J. Phys.: Condens. Matter **22**, 035403 (2010).

[38] E. Granado, J. C. Cezar, C. Azimonte, J. Gopalakrishnan, and K. Ramesha, Electronic structure of Fe and magnetism in the 3*d*/5*d* double perovskites Ca_2FeReO_6 and Ba_2FeReO_6, Phys. Rev. B **99**, 195118 (2019).

[39] S. Seigel and S. L. Quimby, The variation of Young's modulus with magnetization and temperature in nickel, Phys. Rev. **49**, 663 (1936).

[40] J. Chrosch and E. K. H. Salje, Temperature dependence of the domain wall width in $LaAlO_3$, J. Appl. Phys. **85**, 722 (1999).

[41] S. Wenyuan, S. Huimin, W. Yening, and L. Baosheng, Internal friction associated with domain walls and ferroelastic phase transition in LNPP, J. Phys. Colloques **46**, C10-609 (1985).

[42] W. Yening, S. Wenyuan, C. Xiaohua, S. Huimin, and L. Baosheng, Internal friction associated with the domain walls and the second-order ferroelastic transition in LNPP, Phys. Stat. Sol. **102**, 279 (1987).

[43] E. K. H. Salje, *Phase Transitions in Ferroelastic and Co-elastic Crystals* (Cambridge University Press, Cambridge, 1991).

[44] M. A. Carpenter, A. Buckley, P. A. Taylor, and T. W. Darling, Elastic relaxations associated with the *Pm*-3*m*–*R*-3*c* transition in $LaAlO_3$: III. Superattenuation of acoustic resonances, J. Phys.: Condens. Matter **22**, 035405 (2010).

[45] J. F. Scott, E. K. H. Salje, and M. A. Carpenter, Domain Wall Damping and Elastic Softening in $SrTiO_3$: Evidence for Polar Twin Walls, Phys. Rev. Lett. **109**, 187601 (2012).

[46] R. J. Harrison and S. A. T. Redfern, The influence of transformation twins on the seismic-frequency elastic and anelastic properties of perovskite: Dynamical mechanical analysis of single crystal $LaAlO_3$, Phys. Earth Planet. Int. **134**, 253 (2002).

[47] S. A. T. Redfern, C. Wang, J. W. Hong, G. Catalan, and J. F. Scott, Elastic and electrical anomalies at low-temperature phase transitions in $BiFeO_3$, J. Phys.: Condens. Matter **20**, 452205 (2008).

[48] W. Schranz, P. Sondergeld, A. V. Kityk, and E. K. H. Salje, Dynamic elastic response of $KMn_{1-x}Ca_xF_3$: Elastic softening and domain freezing, Phys. Rev. B **80**, 094110 (2009).

[49] E. K. H. Salje and H. Zhang, Domain boundary engineering, Phase Trans. **82**, 452 (2009).

[50] J. Navarro, Ll. Balcells, F. Sandiumenge, M. Bibes, A. Roig, B. Martinez, and J. Fontcuberta, Antisite defects and magnetoresistance in Sr_2FeMoO_6 double perovskite, J. Phys.: Condens. Matter **13**, 8481 (2001).

[51] J. Lindén, M. Karppinen, T. Shimada, Y. Yasukawa, and H. Yamauchi, Observation of antiphase boundaries in Sr_2FeMoO_6, Phys. Rev. B **68**, 174415 (2003).

[52] T.-T. Fang, Reassessment of the role of antiphase boundaries in the low-field magnetoresistance of Sr_2FeMoO_6, Phys. Rev. B **71**, 064401 (2005).

[53] X. Z. Yu, T. Asaka, Y. Tomioka, C. Tsuruta, T. Nagai, K. Kimoto, Y. Keneko, Y. Tokura, and Y. Matsui, TEM study of the influence of antisite defects on magnetic domain structures in double perovskite Ba_2FeMoO_6, J. Electron Microsc. **54**, 61 (2005).

[54] X. Z. Yu, T. Asaka, Y. Tomioka, Y. Kaneko, M. Uchida, J. P. He, T. Nagai, K. Kimoto, Y. Matsui, and Y. Tokura, Pinning effect of the antiphase and grain boundaries on magnetic domains in double perovskite A_2FeMoO_6, J. Magn. Magn. Mater. **310**, 1572 (2007).

[55] T.-W. Lim, S.-D. Kim, K.-D. Sung, Y.-M. Rhyim, H. Jeen, J. Yun, K.-H. Kim, K.-M. Song, S. Lee, S.-Y. Chung *et al.*, Insights into cationic ordering in Re-based double perovskite oxides, Sci. Rep. **6**, 19746 (2016).

[56] D. Choudhury, P. Mandal, R. Mathieu, A. Hazarika, S. Rajan, A. Sundaresan, U. V. Waghmare, R. Knut, O. Karis, P. Nordblad, and D. D. Sarma, Near-Room-Temperature Colossal Magnetodielectricity and Multiglass Properties in Partially Disordered La_2NiMnO_6, Phys. Rev. Lett. **108**, 127201 (2012).

[57] J. P. Palakkal, C. R. Sankar, A. P. Paulose, and M. R. Varma, Hopping conduction and spin glass behavior of La_2FeMnO_6, J. Alloys Compd. **743**, 403 (2018).

[58] M. Nasir, M. Khan, S. A. Agbo, S. Bhatt, S. Kumar, and S. Sen, Evidence of cluster-glass and Griffiths-like phases in partially ordered La_2FeMnO_6 double perovskite, J. Phys. D: Appl. Phys. **53**, 375003 (2020).

[59] M. A. Carpenter, D. Pesquera, D. O'Flynn, G. Balakrishnan, N. Mufti, A. A. Nugroho, T. T. M. Palstra, M. Mihalik, Jr., M. Mihalik, M. Zentkova *et al.*, Strain relaxation dynamics of multiferroic orthorhombic manganites, J. Phys.: Condens. Matter **33**, 125402 (2021).

[60] O. Bidault, M. Maglione, M. Actis, M. Kchikech, and B. Salce, Polaronic relaxation in perovskites, Phys. Rev. B **52**, 4191 (1995).